NEUROSCIENCE

Repopulating retinal microglia restore endogenous organization and function under CX3CL1-CX3CR1 regulation

Yikui Zhang,[1,2]* Lian Zhao,[1]* Xu Wang,[1] Wenxin Ma,[1] Adam Lazere,[1] Hao-hua Qian,[3] Jun Zhang,[4] Mones Abu-Asab,[5] Robert N. Fariss,[6] Jerome E. Roger,[7,8] Wai T. Wong[1]†

Microglia have been discovered to undergo repopulation following ablation. However, the functionality of repopulated microglia and the mechanisms regulating microglia repopulation are unknown. We examined microglial homeostasis in the adult mouse retina, a specialized neural compartment containing regular arrays of microglia in discrete synaptic laminae that can be directly visualized. Using in vivo imaging and cell-fate mapping techniques, we discovered that repopulation originated from residual microglia proliferating in the central inner retina that subsequently spread by centrifugal migration to fully recapitulate pre-existing microglial distributions and morphologies. Repopulating cells fully restored microglial functions including constitutive "surveying" process movements, behavioral and physiological responses to retinal injury, and maintenance of synaptic structure and function. Microglial repopulation was regulated by CX3CL1-CX3CR1 signaling, slowing in CX3CR1 deficiency and accelerating with exogenous CX3CL1 administration. Microglial homeostasis following perturbation can fully recover microglial organization and function under the regulation of chemokine signaling between neurons and microglia.

INTRODUCTION

Our understanding of the function of the healthy adult central nervous system (CNS) has been enlarged by discoveries on how microglia, the primary resident immune cell type, are maintained as a constituent population in adulthood (*1*) and how these cells contribute to ongoing homeostatic activities in the brain (*2*). Recent work has uncovered the intrinsic homeostasis of microglia in the adult brain; depletion of brain microglia via multiple experimental systems has been found to trigger the ability of the brain to generate a rapid recolonization and repopulation by myeloid cells (*3*). This homeostatic response in the microglial compartment is significant because it reveals the constitutive requirement for microglia in the CNS, as well as the mechanisms that specify the precise distribution and morphology of microglia in the neural parenchyma. Although microglial repopulation has been described in the brain (*4*, *5*) and spinal cord (*6*), the functional capabilities of these replacement cells and the underlying mechanisms governing the repopulating process across the CNS have not been elucidated, largely due to difficulties in observing and functionally assessing microglia in vivo using noninvasive methods that do not themselves affect microglial responses.

The retina is one part of the CNS that has the advantage of being accessible to direct noninvasive longitudinal inspection by in vivo fundus imaging (*7*) and to the evaluation of physiological function by electroretinography (ERG) (*8*). In addition, microglia in the retina demonstrate a uniquely structured organization, appearing as parallel mosaics of horizontally ramified cells concentrated in the inner and outer plexiform layers (IPL and OPL, respectively), each with its own local density and arrangement of microglia (*9*). Under physiological conditions, retinal microglia are constitutively required in the structural and functional maintenance of synapses in the adult retina (*10*), allowing ERG measurements to serve as a readout for constitutive microglial function. Hence, the retinal system constitutes a unique system permitting insightful analysis into the nature, dynamics, and functional significance of microglial homeostasis, and into mechanisms involved in the organizational and functional recovery in microglial repopulation. The mechanisms underlying the reestablishment of microglial organization and function in the neural parenchyma likely involve neuron-microglia signaling mechanisms, particularly neuronally derived chemokine signaling (*11*). CX3CL1, or fractalkine, is a neuronally derived chemokine that signals to its cognate microglia-expressed receptor, CX3CR1, and has been found to guide developmental microglial colonization in the brain (*12*) and to modulate maturation of microglial functions (*13*). In the adult retina, CX3CL1 is constitutively expressed by retinal neurons (*14*), and CX3CL1-CX3CR1 signaling actively regulates ongoing microglial "surveying" process motility (*15*) and maintains the normal distribution of microglia in the retina (*16*).

Here, by directly visualizing microglial repopulation occurring in the adult retina, we discovered that microglial repopulation following depletion progresses as concomitant cellular proliferation and migration occurring in situ which propagates as a centrifugal wave across the retina. We found that this repopulation process not only restores microglial numbers but also quantitatively recapitulates local laminar microglial density and morphological parameters of individual microglial cells. Significantly, repopulating microglia demonstrated functional capabilities similar to those of endogenous microglia in terms of their surveying behavior, response to light injury, and their ability to maintain synapses and sustain electrophysiological responses to light, indicating full restoration of microglial functions during homeostasis. In addition, we uncovered evidence that constitutive CX3CL1-CX3CR1 signaling regulates microglial repopulation in the retina by potentiating the proliferation and morphological maturation of repopulating cells, underscoring neuron-microglial communication as an important mode for microglial homeostatic regulation.

[1]Unit on Neuron-Glia Interactions in Retinal Disease, National Eye Institute, National Institutes of Health, Bethesda, MD 20892, USA. [2]The Eye Hospital, School of Ophthalmology & Optometry, Wenzhou Medical University, Wenzhou 325027, China. [3]Visual Function Core, National Eye Institute, National Institutes of Health, Bethesda, MD 20892, USA. [4]Synaptic Physiology Section, National Institute of Neurological Disorders and Stroke, National Institutes of Health, Bethesda, MD 20892, USA. [5]Section on Histopathology, National Eye Institute, National Institutes of Health, Bethesda, MD 20892, USA. [6]Biological Imaging Core, National Eye Institute, National Institutes of Health, Bethesda, MD 20892, USA. [7]Centre d'Etude et de Recherche Thérapeutique en Ophtalmologie (CERTO), Retina France, Orsay, France. [8]Paris-Saclay Institute of Neuroscience, CNRS, Université Paris-Sud, Université Paris-Saclay, Orsay, France.
*These authors contributed equally to this work.
†Corresponding author. Email: wongw@nei.nih.gov

These findings are of potential therapeutic significance; because chronic microglial changes have been causally associated with neurodegeneration in multiple CNS pathologies (*17*), the ability to understand and modulate microglial homeostasis can facilitate the reconstitution of the CNS with healthy functional microglia following the depletion of pathologic microglia as a means to improve disease outcomes (*18*). Our results here help elucidate the nature of the repopulation process and its regulation by neuron-microglia signaling and can be used to support the development of this novel therapeutic strategy.

RESULTS

Microglial distribution after depletion is restored by a center-to-peripheral, interlaminar spread of repopulating cells

Microglia repopulation following depletion is a phenomenon described in the brain and spinal cord (*4*–*6*) but is yet uncharacterized in the retina. The mature retina in primate and rodent systems demonstrates a unique laminar organization in which microglia are distributed in a regular mosaic pattern within the retinal plexiform layers (*19*), where they perform constitutive maintenance of synaptic structure and function (*10*). We investigated whether and how microglial homeostasis is maintained in the adult retina following microglial depletion as induced by two separate models: (i) a genetic model in which tamoxifen-inducible Cre recombinase expressed in myeloid cells under the control of the *CX3CR1* promoter enabled the microglia-specific expression of diphtheria toxin A (DTA) in the retina (termed the *CX3CR1*^{CreER}*-DTA* model) (*20*), and (ii) a pharmacological model in which PLX5622, a small-molecule inhibitor of the colony-stimulating factor 1 receptor (CSF1R), was used to inhibit microglial CSF1R signaling required for microglial survival (*21*).

Before microglial depletion, 2-month-old *CX3CR1*^{CreER}*-DTA* transgenic mice showed microglial numbers and spatial distributions similar to those of age-matched wild-type controls (*10*). Upon DTA induction, retinal microglia were rapidly and substantially depleted, falling to 0.58 ± 0.11% of baseline levels 9 days following the last tamoxifen dose [days post-tamoxifen gavage (DPG)] (Fig. 1, A to C). Repopulating Iba1$^+$ cells first increased in number in the central retina close to the optic nerve head and then spread progressively in a centrifugal direction toward the peripheral retina (Fig. 1, D to F), extending to all retinal areas by 30 days DPG and reestablishing baseline microglial densities by 150 days DPG (Fig. 1, G and H). Retinal levels of microglia-enriched genes recovered progressively with time following depletion, indicating that repopulating cells expressed distinguishing genes similar to those of endogenous microglia (Fig. 1I). Apart from the early localization of repopulating cells in the central retina, no separate localized microglial clusters were observed as described in the brain (*4*).

Because microglia in the retina are arranged in parallel mosaic arrays found predominantly in the IPL and OPL (Fig. 2A), we monitored the recovery of this laminar organization of microglia during repopulation. Repopulating microglia first appeared in the IPL, increasing rapidly in number such that by 16 days DPG, a supranormal density (154 ± 13% of baseline numbers) of microglia was measured in the IPL (Fig. 2, A to C), whereas microglia in the OPL were still sparse. Subsequently, microglial numbers in the IPL decreased and those in the OPL conversely increased. This trend continued until baseline microglial numbers in both the IPL and the OPL were reestablished at 150 days DPG (Fig. 2C). These reciprocal changes indicated that repopulating microglia were initially generated in excess in the IPL, which were then redistributed to the OPL to restore original microglial numbers in each lamina. Transitory movement of microglia in the vitreal-to-scleral direction from the IPL to the OPL was indicated by a transient increase in the proportion of microglial somata found between the IPL and the OPL (that is, interplexiform microglia) at 60 days DPG during the redistribution process (Fig. 2D).

In the alternative PLX5622 model in which CSF1R blockade by PLX5622 administration was used to induce microglial depletion in wild-type mice, a centrifugal center-to-peripheral, IPL-to-OPL pattern of repopulation that fully reestablished baseline total and laminar microglial densities in the retina was similarly observed (fig. S1). The time taken to reestablish baseline microglia distribution (30 days following PLX5622 cessation) was less than that in the *CX3CR1*^{CreER}*-DTA* transgenic model.

Repopulating microglia undergo progressive ramification to reestablish morphological features of endogenous microglia

Repopulating retinal microglia initially demonstrated simple dendritic morphologies in early repopulation (day 16 DPG in the *CX3CR1*^{CreER}*-DTA* model) that increased in ramification over time (fig. S2A). Three-dimensional morphological analyses using Imaris software revealed that dendritic arbors of repopulating cells in both the IPL and the OPL lamina increased progressively (i) in morphological complexity (measured as the mean number of branching points per cell), (ii) in process elaboration (measured as the mean total length of processes per cell), and (iii) in overall size (measured as the volume subtended by the dendritic field arbor) (fig. S2B). At the time point when microglial densities have returned to baseline values (150 DPG), all morphological parameters have also recovered to baseline values (that is, those of endogenous retinal microglia before depletion). Analyses of repopulating microglia using the PLX5622 model also revealed similar features of morphological maturation (fig. S3).

As described in the brain (*4*, *5*), repopulating microglia in the retina demonstrated positivity for markers of activation [isolectin B4 (IB4) and CD68] early during the repopulation process, which were subsequently down-regulated; these patterns were observed in both the *CX3CR1*^{CreER}*-DTA* model (fig. S4, A to C) and the PLX5622 model (fig. S5, A to C). In early repopulation, a substantial fraction of IB4$^+$ and CD68$^+$ repopulating microglia were co-labeled with Ki67, a marker of cellular proliferation, indicating active proliferation in repopulating cells. Later in the process when repopulation was more complete, Ki67 immunopositivity decreased to very low levels or was absent (figs. S4, D and E, and S5, D and E).

CX3CR1-expressing residual endogenous microglia undergo rapid proliferation and intraretinal migration

In the brain, microglial repopulation following depletion has been described as deriving from stem cell–like nestin-positive precursors (*5*) and alternatively from CX3CR1-expressing internal pools of microglia (*4*). In the presence of irradiation or CNS injury, bone marrow–derived monocytes from peripheral sources have also been found to take up the microglial niche (*4*). To investigate whether the repopulating microglia in the retina originate from a residual internal pool and not from systemic monocytes, we performed a cell-fate mapping technique that distinguishes endogenous microglia from monocytes based on their different life spans (*20*). *CX3CR1*$^{CreER/+}$ transgenic mice were crossed with mice with a loxP-flanked STOP codon upstream of sequences coding for tdTomato (tdT) that had been inserted into the *Gt*(*ROSA*)*26Sor* locus; tamoxifen was administered to induce tdT expression in

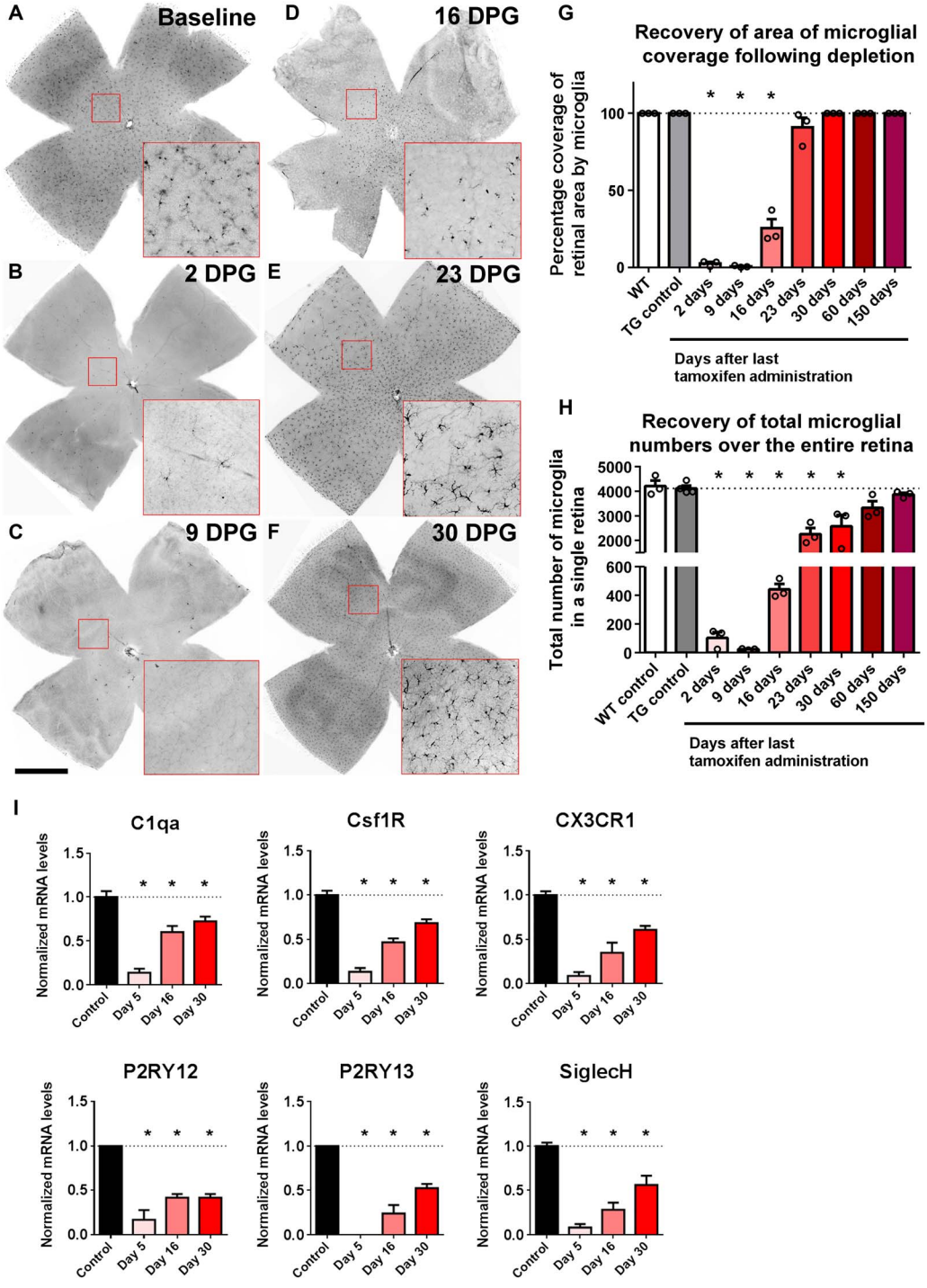

Fig. 1. Microglial repopulation of the adult mouse retina following genetic depletion occurs in a progressive center-to-peripheral direction originating from the optic nerve head. (**A** to **F**) The overall distribution of Iba1-immunopositive cells was analyzed in flat-mounted retinal preparations; insets (red boxes) show repopulating cells at high magnification. (A) Young adult (2 months old) *CX3CR1*^{CreER}*-DTA* transgenic mice demonstrated a wild-type–like distribution of microglia in the retina under baseline conditions. (B and C) Following the administration of oral tamoxifen (500 mg/kg per dose, two doses administered 1 day apart) to deplete the retina of microglia, few microglia remained at 2 to 9 days DPG. (D to F) Progressive repopulation of the retina occurred thereafter in a central-to-peripheral direction extending to all topographical areas of the retina. Scale bar, 1 mm. (**G**) The percentage of the total retinal area occupied by Iba1$^+$ cells was measured at different times following tamoxifen-induced depletion. Repopulating cells extended to all retinal areas by 30 DPG. (**H**) The total number of Iba1$^+$ cells in the retina following depletion recovered progressively to reach the number present before depletion. (**I**) mRNA expression levels of microglia-enriched genes in the retina, assessed using next-generation sequencing, demonstrated marked decreases at 5 DPG, followed by progressive recovery at 16 and 30 DPG. mRNA levels of each species were normalized to the mean level of expression in the controls. [Graphical data in (G), (H), and (I) are presented as means ± SEM; one-way analysis of variance (ANOVA) and Sidak's multiple comparison test, $n = 3$ animals of mixed sex at each time point, except $n = 4$ in the transgenic (TG) control group. Asterisks (*) indicate comparisons with control for which $P < 0.05$.]

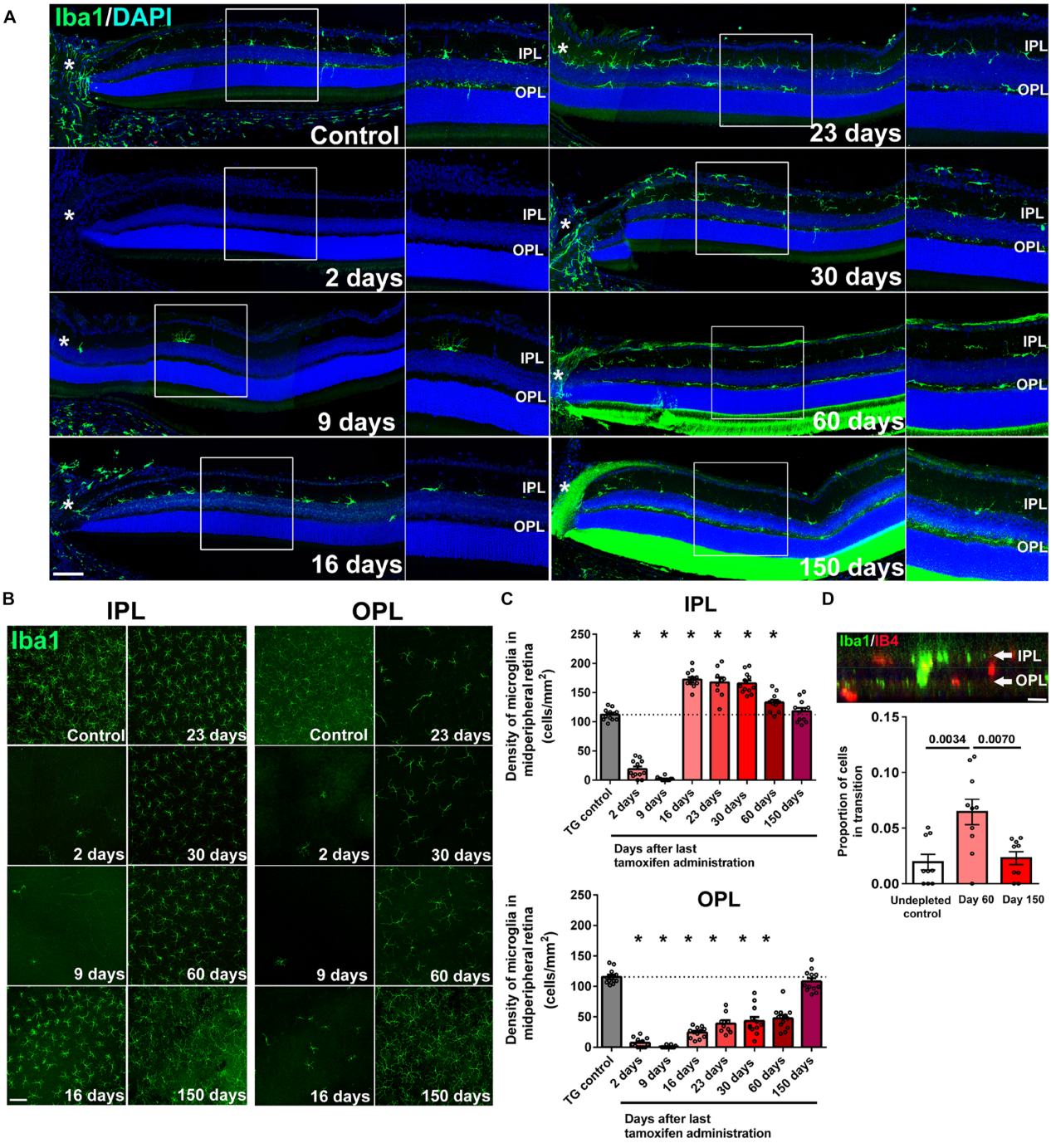

Fig. 2. Microglial repopulation in the retina involves microglial migratory transit in an inner-to-outer direction to reestablish local laminar densities in each plexiform layer. (**A**) The spatial pattern of microglia recolonization in separate retinal lamina following depletion was analyzed in retinal sections; asterisks (*) indicate the optic nerve head, and insets show high-magnification views of the IPL and OPL. Near-complete absence of retinal microglia in all retinal layers was observed at 2 DPG, with few Iba1$^+$ cells found only in the IPL near the optic nerve head. At 16 DPG, significant numbers of Iba1$^+$ cells were present in the IPL but were largely absent in the OPL. Recolonization of the OPL progressed at later time points from central to peripheral retinal areas. Scale bar, 50 μm. DAPI, 4′,6-diamidino-2-phenylindole. (**B**) Repopulation dynamics of Iba1-labeled microglia in the IPL and OPL were analyzed additionally in retinal flat-mounts using confocal microscopy at midpoint between the optic nerve head and the retinal periphery. Scale bar, 100 μm. (**C**) Quantitative analysis of microglial density demonstrated a rapid repopulation of the IPL at 16 DPG (top) that exceeded the numbers of endogenous microglia present at baseline (TG control). At subsequent time points, microglial density in the IPL slowly declined to baseline levels by 150 DPG. Microglial repopulation of the OPL (bottom) demonstrated a slow progressive recovery, reaching baseline levels by 150 DPG. (**D**) The proportion of interplexiform Iba1$^+$ cells (with somata located between IPL and OPL lamina), expressed as a fraction of all microglial cells in the imaging field, was assessed at (i) baseline (before depletion), (ii) midway through the repopulation process (60 DPG), and (iii) upon the reattainment of baseline distribution (150 DPG). Scale bar, 10 μm. The proportion of interplexiform Iba1$^+$ cells was significantly greater at 60 DPG than at other time points, indicating an inner-to-outer migration of microglia during repopulation. Graphical data in (C) and (D) are presented as means ± SEM (n = 12 imaging retinal fields from three animals of mixed sex at each time point; P values were derived from one-way ANOVA and Sidak's multiple comparison test).

both CX3CR1-expressing monocytes and microglia. tdT expression was durable in long-lived microglia but transient in short-lived monocytes because these were subject to replacement by tdT^- monocytes with time. Microglial depletion using PLX5622 was carried out in adult *CX3CR1*$^{CreER/+}$*:tdT* mice 2.5 to 3 months after tamoxifen administration to allow for complete monocyte turnover, and the tdT expression status of repopulating $Iba1^+$ microglia was monitored. Immediately following depletion, in vivo fundus imaging demonstrated a few tdT^+ microglia located near the optic nerve head; with time, tdT^+ microglial numbers increased prominently to colonize the retina, indicating that an internal pool of residual CX3CR1-expressing microglia significantly contributed to repopulating cells (Fig. 3A). Immunohistochemical analysis of repopulated retina at day 30 corroborated the finding that nearly all $Iba1^+$ microglia were tdT^+, indicating that residual endogenous microglia were the primary source of repopulating cells, with little contribution from the infiltration of peripheral tdT^- monocytes (Fig. 3, B and C). To support this conclusion, we examined the contribution of CCR2-expressing monocytes to repopulating cells using *CCR2*$^{RFP/+}$ transgenic mice in which $CCR2^+$ monocytes were labeled with RFP (*22*). In both the PLX5622-mediated and the *CX3CR1*$^{CreER/+}$*-DTA* models of microglial depletion, no $CCR2^+$ monocytes were detected among repopulating cells during the early phase of repopulation when newly infiltrating monocytes, if present, were likely to be found (Fig. 3, D and E). These results supported the conclusion that monocytic infiltration did not significantly contribute to microglial homeostasis in the retina.

To visualize the process of retinal repopulation by residual microglia, we performed in vivo time-lapse fundus imaging in *CX3CR1*$^{+/GFP}$ transgenic animals containing green fluorescent protein (GFP)–labeled microglia to track the progression of microglial repopulation. At 5 days following PLX5622-mediated depletion, repopulating cells were sparse and were found near the optic nerve head (Fig. 3F). Time-lapse images captured every 1 to 1.5 hours showed that these early cells with simple morphologies demonstrated rapid migration within the horizontal plane of the retina, moving at mean horizontal velocities of ≈2 μm/min (Fig. 3F and movie S1). Manual tracking of microglial migration showed irregular, wandering tracks that were not strictly confined to a radial center-to-peripheral axis; net displacements of repopulating cells averaged ≈1.5 μm/min. In addition, multiple repopulating microglia underwent binary division to form pairs of daughter cells that subsequently migrated apart; scoring of the number of binary divisions observed across recordings at this time point enabled an estimate of 0.624 cell divisions per cell per day. By day 12 following depletion, the density of microglia in the central retina had increased significantly (Fig. 3G); time-lapse imaging at this time point revealed decreased microglial migration and division rates relative to those at day 5, indicating that migration and division slowed as microglial density approached baseline values (Fig. 3, H and I, and movie S2).

Repopulated retinal microglia recapitulate multiple functional features of endogenous microglia

Next, we examined whether repopulated microglia, in restoring the overall distribution, local density, and precise morphology of endogenous microglia, were able to recapitulate the full functions of endogenous microglia. Akin to microglia in the brain, retinal microglia under endogenous conditions demonstrate constitutive dynamic process motility that is highly responsive to signals such as extracellular adenosine triphosphate (ATP) (*23*). We performed microglial depletion using PLX5622 in young 10-week adult *CX3CR1*$^{GFP/+}$ transgenic mice and allowed repopulation to occur. Using ex vivo time-lapse confocal imaging in retinal explants under standardized conditions, we recorded and compared process motility in endogenous microglia (in age-matched *CX3CR1*$^{GFP/+}$ transgenic mice that had not undergone microglial depletion) versus repopulated microglia at day 60 of repopulation. We found that repopulated microglia demonstrated baseline dynamic process movements that were similar in nature and in their rate of process movement to those found in endogenous microglia (Fig. 4A and movie S3). Repopulated microglia also responded to the application of exogenous ATP (1 mM) with an elaboration of processes and an increase in process motility that were statistically identical to that demonstrated by endogenous microglia. Because microglial motility is subject to chemokine, neurotransmitter, and ATP-mediated regulation in the retina (*15*, *24*), these findings indicated that these signaling mechanisms were likely recapitulated in repopulated microglia, enabling them to restore homeostasis of microglial "surveillance" in the retina.

In addition to maintenance functions in the healthy CNS, microglia demonstrate functional responses to neural injury by overt migration to the injury site and transition to an activated phenotype (*25*). In the retina, microglia respond to photoreceptor injury induced by acute light exposure by migration from the inner to the outer retina, expression of activation markers, and increases in proinflammatory cytokine expression (*26*). We found that repopulated microglia in the retina demonstrated injury responses to a standardized light injury model that were similar to those in endogenous retinal microglia, in terms of migration to the subretinal space, transition from a ramified to an amoeboid morphology, and the expression of CD68, a marker of activation (Fig. 4B). Levels of proinflammatory cytokines induced in the retina following light injury, which originate predominantly from activated microglia, were also statistically similar between retinas containing endogenous microglia and those containing repopulated microglia (Fig. 4C). These findings indicated that repopulated microglia recapitulated functional injury responses of endogenous microglia in the retina.

We have previously found that endogenous retinal microglia performed constitutive maintenance of synaptic integrity; in the absence of microglia, ERG amplitudes demonstrated progressive decrements with time that were correlated with degenerative ultrastructural changes in synaptic structure (*10*). To evaluate the ability of repopulated microglia to carry out this function, we performed microglial depletion in *CX3CR1*^{CreER}*-DTA* animals for 30 days to induce a decrement in ERG amplitudes and then divided the animals into the following subgroups: (i) continued depletion for another 30 days, (ii) repopulation for 30 days, and (iii) repopulation for 60 days. Comparison of ERG amplitudes in animals subjected to continuous depletion for 60 days with those in animals allowed to undergo repopulation (for 30 or 60 days) revealed significantly greater ERG amplitudes in repopulated animals, indicating that repopulated microglia were capable of conducting endogenous maintenance of ERG responses (Fig. 5). However, ERG amplitudes in repopulated retinas did not fully recover to baseline predepletion levels, indicating that ERG decrements resulting from sustained depletion may not be fully reversed by repopulating cells.

To examine the effects of microglial repopulation on synaptic maintenance following short-term microglial depletion, we used the PLX5622 model to induce microglial depletion in wild-type animals for 1 week and allowed repopulation to occur over the next 4 weeks. Comparison of ERG amplitudes in these animals with those in animals that were depleted continuously for 5 weeks demonstrated significantly greater ERG amplitudes in repopulated animals; these amplitudes were also statistically similar to those in animals with age-matched endogenous microglia (that is, not subjected to depletion) (fig. S6A), indicating that if repopulation was

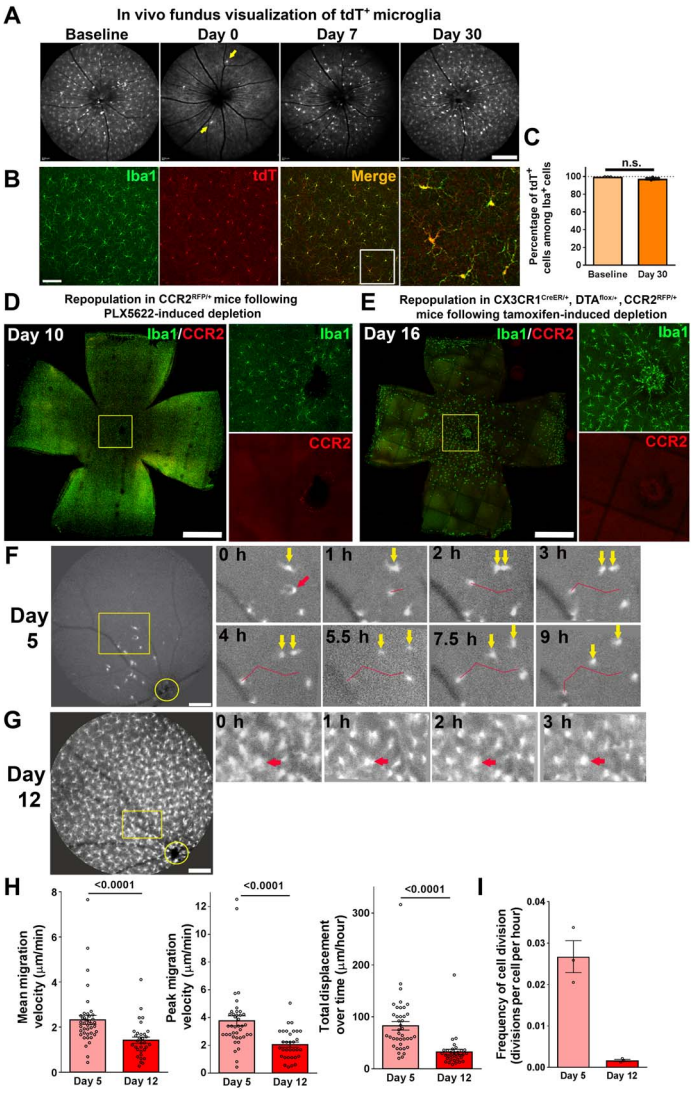

Fig. 3. Iba1$^+$ cells that repopulate the retina following depletion arise from residual endogenous microglia that demonstrate dynamic cellular migration and in situ proliferation. (**A**) Two-month-old *CX3CR1$^{CreER/+}$:Rosa26-flox-STOP-flox-tdTomato* transgenic mice (*CX3CR1 $^{CreER/+}$:tdT* mice) were administered a bolus dose of tamoxifen (two oral gavage doses of 10 mg, 1 day apart) to induce the expression of tdT in CX3CR1-expressing myeloid cells. They were then maintained under standard conditions for 3 months to allow for the turnover and full replacement of circulating monocytes by newly generated tdT$^-$ monocytes. Long-lived endogenous microglia in the retina retained their tdT labeling. In vivo fluorescence fundus images centered on the optic nerve were obtained using a 518-nm excitation laser to detect cells expressing red fluorescent protein (RFP). Fundus images revealed extensive tdT expression in retinal microglia before PLX5622-induced depletion at baseline. Following 1 week of PLX5622 administration (day 0), a few tdT-expressing microglia remained (yellow arrows). Fundus imaging at days 7 and 30 demonstrated a gradual repopulation of the retina in a center-to-periphery direction by tdT$^+$ microglia, indicating residual microglia as the source of repopulating cells. Scale bar, 200 μm. (**B**) Analysis of flat-mounted retina at day 30 of repopulation showed that nearly all Iba1$^+$ (green) repopulating cells were also tdT$^+$ (red). The boxed area in the merged image is shown on the right at higher magnification. Scale bar, 100 μm. (**C**) Quantification of the proportion of Iba1$^+$ cells that were also tdT$^+$ at baseline (before tamoxifen administration) and at day 30 following depletion indicated that close to 100% of Iba1$^+$ repopulating microglia were tdT$^+$ ($n = 5$, 3 animals at baseline and at day 30, respectively). n.s., not significant. (**D**) To detect the contribution of CCR2-expressing monocytes to repopulating Iba1$^+$ cells, *CCR2$^{+/RFP}$* mice containing RFP$^+$ monocytes were subjected to PLX5622-induced depletion and analyzed at day 10 following depletion. No expression of CCR2 was noted in repopulating Iba1$^+$ microglia, either at the optic nerve head (shown in the inset at high magnification) or elsewhere in the retina. (**E**) Microglial repopulation at day 16 of the genetic depletion model involving *CX3CR1$^{Cre/+}$:CCR2$^{+/RFP}$* mice similarly consisted of Iba1$^+$ repopulating cells that were negative for CCR2 expression. Scale bars, 1 mm (D and E). (**F**) Eleven-week-old *CX3CR1$^{+/GFP}$* transgenic mice with GFP-labeled microglia were administered PLX5622 for 7 days to deplete retinal microglia. Time-lapse in vivo fundus imaging was performed at 5 days (top) and 12 days (bottom) following PLX5622 cessation. At day 5 of repopulation, few GFP$^+$ cells were observed in the central retina near the optic nerve head (yellow circle). Time-lapse images taken every 1 to 1.5 hours revealed dynamic and prominent horizontal migration of GFP$^+$ cells across the retina (the red arrow indicates a migrating cell with the red line indicating its migratory track). Binary cellular divisions of repopulating microglia followed by the separation of the two daughter cells (yellow arrows) were also observed. Scale bar, 250 μm. (**G**) At day 12 of repopulation, when microglial density in the central retina had increased significantly, migration and cellular division were slowed relative to that at day 5 (red arrows show a cell with a relatively stable position). Scale bar, 250 μm. (**H**) Quantitative comparison of dynamic migration of individual repopulating microglia, demonstrating higher mean migration velocity, higher peak velocity of movement, and greater net displacement of cell position at day 5 when repopulating microglia were lower in density, relative to corresponding values at day 12 (*P* values from Mann-Whitney test; $n = 40$ and 32 cells from 4 and 3 animals at days 5 and 12, respectively). (**I**) The frequency of dynamic cell divisions was higher early in the repopulation process at day 5 relative to that at day 12 ($n = 4$ and 3 recordings from 4 and 3 animals at days 5 and 12, respectively).

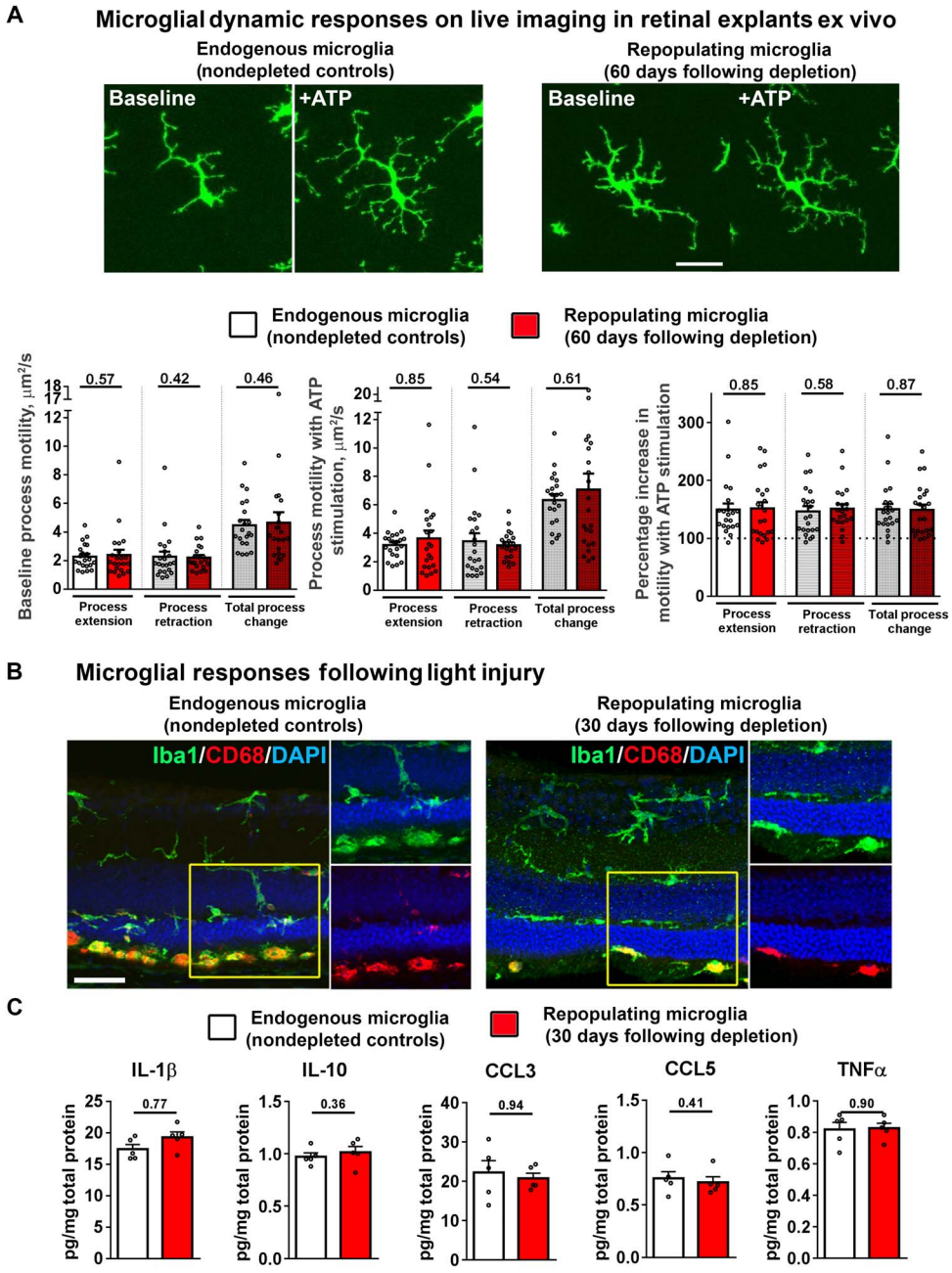

Fig. 4. Repopulating microglia recapitulate endogenous microglial functions of dynamic process motility and response to injury signals. Ten-week-old *CX3CR1*$^{+/GFP}$ transgenic mice were administered PLX5622 for 1 week to induce depletion of retinal microglia and then allowed to undergo full repopulation for 60 days. Age-matched *CX3CR1*$^{+/GFP}$ mice maintained on a standard diet served as controls. (**A**) Ex vivo live-cell time-lapse imaging was performed in retinal explants to monitor process dynamics of repopulated microglia in PLX5622-fed mice versus endogenous microglia in control mice. Repopulated microglia relative to endogenous microglia demonstrated similar process motility at baseline and increased process motility and process elaboration in response to ATP stimulation (1 mM bath application). Scale bar, 30 μm. Quantitative analysis demonstrated that process motility measures, in terms of rates of process extension and process retraction, at baseline and in response to ATP stimulation were statistically similar between endogenous microglia (white bars) and repopulated microglia (red bars) (*P* values from Mann-Whitney test; control group = 21 cells from 9 recordings, repopulation group = 23 cells from 11 recordings, 4 animals in each group). (**B** and **C**) Response of endogenous versus repopulated cells in an in vivo model of light-induced injury. Wild-type mice were subjected to transient depletion (7 days of PLX5622 administration) and allowed to undergo full repopulation for 30 days and then subjected to light-induced photoreceptor injury. Nondepleted age-matched wild-type mice served as controls. Histological analysis (B) showed that repopulated Iba1$^+$ cells, such as endogenous microglia, responded to photoreceptor injury by migration into the outer retina and the subretinal space and by up-regulation of CD68 expression (insets show the presence of subretinal Iba1$^+$ and CD68$^+$ cells in both groups). Scale bar, 40 μm. (C) Levels of post-injury inflammatory cytokines [interleukin (IL)-1β, IL-10, C-C motif chemokine ligand 3 (CCL3), CCL5, and tumor necrosis factor–α (TNFα)] were similarly elevated in retinas containing endogenous microglia versus repopulated cells (*P* > 0.05 for all comparisons; Mann-Whitney test, *n* = 5 retina from individual animals of mixed sex per group).

allowed to occur promptly after depletion, repopulated microglia were able to maintain ERG responses at the same level as endogenous microglia. This rescue effect was correlated with the prevention of degenerative changes in the ultrastructure of IPL and OPL synapses in retinas in which repopulation occurred, whereas these changes were present in retinas subjected to 5 weeks of continuous depletion (fig. S6B).

Microglial repopulation is regulated by CX3CR1 signaling

The robustness and dynamic nature of the microglial repopulation process in the retina indicated the existence of intrinsic regulatory mechanisms enabling a full and precise recapitulation of microglial distribution, structure, and function. Because constitutive chemokine communication in the retina in the form of CX3CL1-CX3CR1 signaling has been found to regulate microglial distribution (*16*), process motility (*15*), and activation (*27*), we examined whether microglial repopulation may be influenced by CX3CR1 signaling. We performed PLX5622-mediated depletion in signaling-sufficient *CX3CR1*$^{+/-}$ transgenic mice and their signaling-deficient *CX3CR1*$^{-/-}$ littermates for 7 days and compared microglial repopulation rates. We monitored early repopulation in the first 10 days using in vivo fundus imaging; although the efficiency of microglia depletion was similar between the two genotypes, *CX3CR1*$^{-/-}$ animals demonstrated a significantly slower recovery of microglial numbers at days 7 and 10 (Fig. 6, A and B). We further used histological analyses of microglial density in the OPL to examine repopulation in the later stages; although microglial densities remained significantly lower at day 14 in *CX3CR1*$^{-/-}$ animals, they were statistically similar between the two genotypes following day 32 (Fig. 6, C and D). This difference in microglial densities during early repopulation is likely contributed to by differences in microglial proliferation; the fraction of repopulating microglia that were Ki67-immunopositive at day 14 was significantly lower in *CX3CR1*$^{-/-}$ than in *CX3CR1*$^{+/-}$ animals (Fig. 6E). We also analyzed the rate of morphological maturation in repopulating cells between the genotypes (Fig. 6F). The recovery of morphological parameters, including (i) branch point number (Fig. 6G), (ii) dendritic segment number (Fig. 6H), (iii) total dendritic length (Fig. 6I), and (iv) area of retinal coverage by microglial processes (Fig. 6J), was significantly slower in *CX3CR1*$^{-/-}$

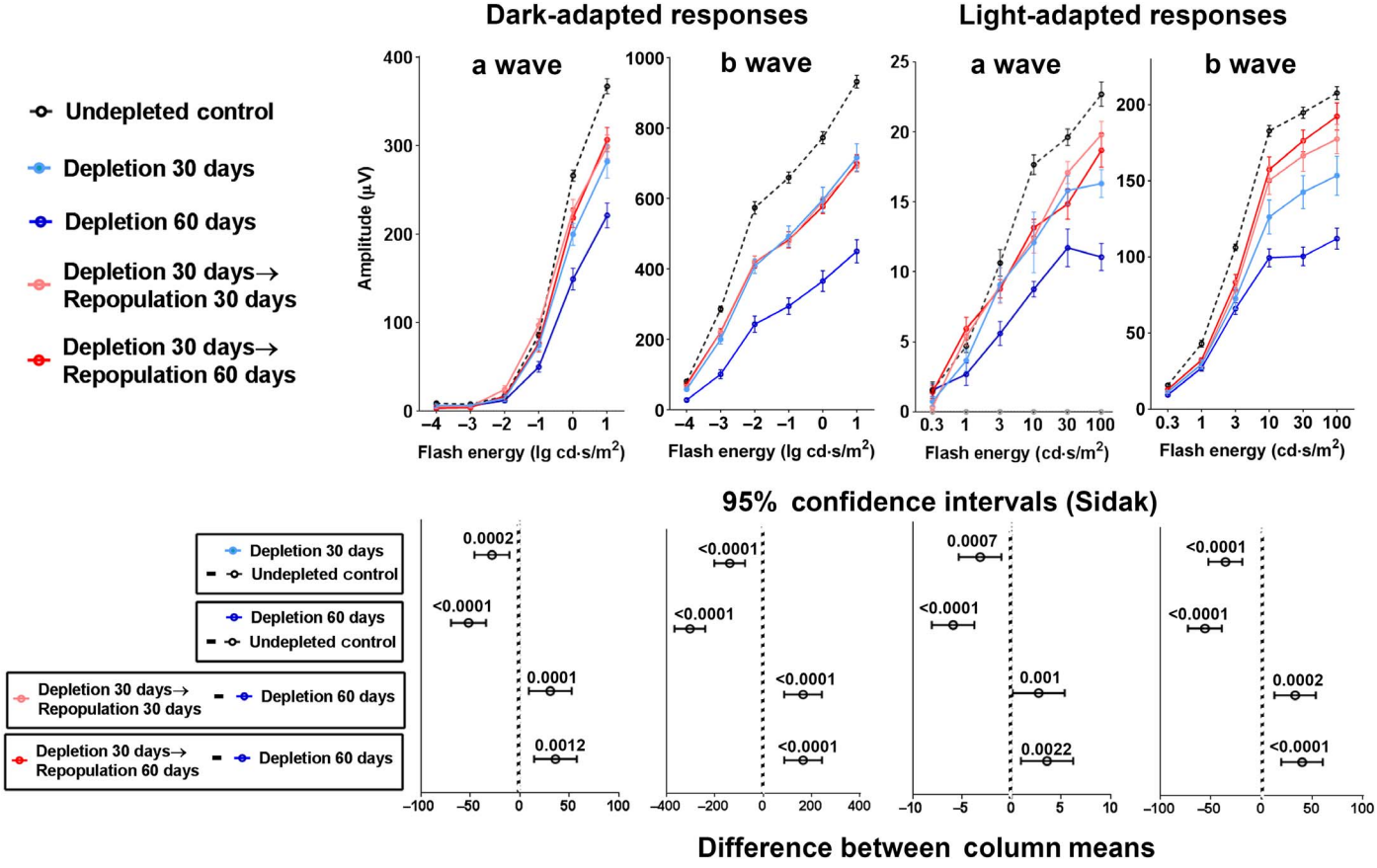

Fig. 5. Microglial repopulation rescues deterioration of retinal function induced by microglia depletion in the *CX3CR1*^{CreER}-*DTA* model. Twelve-week-old *CX3CR1*^{CreER}-*DTA* mice were subjected to sustained microglia depletion for 30 days (light blue line). Following this period, experimental mice were divided into three subgroups: (i) maintained microglial depletion for another 30 days (total of 60 days) (dark blue line), (ii) repopulation for 30 days (pink line), and (iii) repopulation for 60 days (red line). Undepleted *CX3CR1*^{CreER}-*DTA* mice served as controls (black dashed line). Sustained microglial depletion resulted in decreases in ERG responses in the a- and b-wave amplitudes that progressed from 30 to 60 days depletion. In the groups undergoing repopulation, these further decrements in ERG responses were halted and were significantly greater than those in animals undergoing 60 days sustained depletion. Upper panels show ERG amplitudes in all subgroups with data points and error bars indicating mean responses ± SEM. Lower panels show statistical comparisons between subgroups with data points and error bars indicating mean differences and ±95% confidence intervals [error bars not crossing $x = 0$ indicate significant ($P < 0.05$) comparisons]. Two-way ANOVA with Sidak's multiple comparison test was used to calculate P values; $n = 24$ eyes in 12 animals in the control subgroup, and $n = 8$ eyes in 4 animals for all other subgroups.

than in *CX3CR1*$^{+/-}$ animals at day 14. By day 32, however, morphological parameters were similar between genotypes and recapitulated features present in endogenous microglia at baseline.

CX3CL1, the cognate ligand for CX3CR1, is constitutively expressed by retinal neurons under normal conditions (*14*). We did not find that retinal levels of CX3CL1 as analyzed by enzyme-linked immunosorbent assay changed significantly during repopulation relative to baseline levels (day 0, 117 ± 23%; day 7, 89 ± 7%; and day 30, 93 ± 19%; values represent % relative to baseline; mean ± SD; $n = 4$ animals per time point; $P > 0.81$ for all comparisons, Kruskal-Wallis test with Dunn's multiple-comparisons test), indicating that CX3CL1 levels were relatively constant during repopulation, which was consistent with the stable mRNA expression levels of CX3CL1 in the brain during depletion and repopulation (*5*). These findings indicate that CX3CL1 may act as a constitutive signal within the retina that positively regulates the dynamics of repopulation by increasing microglial proliferation and morphological maturation. To investigate the role of CX3CL1 signaling in microglial repopulation, adult *CX3CR1*$^{+/GFP}$ mice, which were depleted with 1 week of PLX5622 administration and then allowed to undergo repopulation, were additionally administered intravitreal recombinant CX3CL1 [1.5 μl injection of 66 ng/μl solution in phosphate-buffered saline (PBS), administered at day 3 of repopulation] in one eye. The contralateral eye was injected with an equal amount of heat-inactivated CX3CL1 in PBS, serving as a control. In vivo fundus imaging and histological analyses in retinal flat mount demonstrated significantly greater numbers of repopulating microglia in CX3CL1-treated eyes relative to control eyes at day 7 of repopulation (fig. S7, A and B). On the contrary, intravitreal injection of CX3CL1 in CX3CR1-deficient mice exerted no significant effect on microglial repopulation (fig. S7B), indicating that this CX3CL1 effect was mediated through the CX3CR1 receptor. Together, these results indicate that CX3CL1-CX3CR1 neuron-microglia chemokine signaling positively regulates microglial repopulation in the retina.

DISCUSSION

Complete homeostatic recovery of microglial organization in the retina following microglial ablation

Here, we find evidence that microglial homeostasis following depletion unfolds in a coordinated manner that involves the proliferation and migration of residual cells to fully recapitulate the high degree of microglial organization unique to the retina. In comparison to other regions of the CNS, microglia in the laminated retina are distributed as horizontally ramified cells arrayed in a regular mosaic pattern in the IPL and OPL, each of which contains specific microglial densities and morphological characteristics. Although previous studies have documented the phenomenon of microglial repopulation following ablation in the brain (*4*, *5*), our findings here show that microglial repopulation is a general phenomenon in the CNS that extends to the retina. In addition, the data here provide a detailed quantitative characterization for the progressive recovery of microglial organization in the retina at the levels of general numbers, specific local distribution in each lamina, and morphological maturation that can serve as a system for elucidating the principles and mechanisms underlying different aspects of microglial homeostasis.

By using either genetic or pharmacological models of microglial ablation, we were able to achieve a near-complete degree of depletion in the retina. Only a small fraction of pre-existing Iba1-expressing microglia remained following ablation that likely represent residual endogenous cells. The reasons why some residual cells remain unablated in these and other depletion models (*3*, *28*) remain unclear and may relate to an increased local drive for microglial survival and proliferation that overcomes the depleting influences as microglial numbers decline. Unlike what had been reported in the brain (*4*), microglial ablation in the retina did not entail increases in proinflammatory cytokines or overt gliosis in retinal macroglia (*10*). In our cell-fate mapping and in vivo retinal imaging experiments, we ascertained that microglial repopulation originated from residual CX3CR1-expressing microglia and that microglial proliferation occurred in situ within the retina proper, rather than arising from CX3CR1-negative stem cell precursors that subsequently differentiated into microglia (*5*). We observed that the proliferation activity was highly up-regulated soon after microglial depletion and subsequently declined in concert with the recovery of microglial numbers. The estimated rates of in situ proliferation obtained from in vivo observations indicate that these were sufficient to regenerate the necessary microglial numbers within the time taken to achieve full repopulation, without the need to invoke additional cellular sources (fig. S8). While circulating monocytes have been reported to infiltrate the retina in the context of retinal disease (*29*), we were unable to detect monocytic contribution to homeostatic replenishment in the uninjured retina, in contrast with models in which the blood-brain barrier may be compromised (*30*).

In addition to proliferation, our findings demonstrate that microglial homeostasis in the retina involves rapid migration of proliferating cells that occurs as a directed wave initiating near the optic nerve head and inner layers of the retina and then spreading centrifugally to more peripheral regions of the retina and into the outer retinal layers. This pattern differs from that seen in the brain, which arises from local clusters of proliferating cells (*4*). Proliferation and migration activities appeared to be highly synchronized in the retina; excessive numbers of microglia were initially generated in the IPL by rapid proliferation, and were subsequently redistributed via migration to achieve the correct final densities in both the IPL and the OPL. These migrating cells were found to home into the correct retinal layers with little mistargeting to regions of the retina where microglia are not typically found (that is, the outer nuclear layer and subretinal space), suggesting the existence of intraretinal cues that guide the direction and destination of migrating microglia. Because they achieved their final positions in the retina, repopulating microglia showed a progressive increase in ramification and process growth that culminated in the reestablishment of microglial organization and coverage in the plexiform layers. Together, these dynamic events indicate a high degree of interaction between neighboring microglial cells and between microglia and their environmental cues, particularly in the synaptic plexiform layers. Future studies are needed to elucidate the mechanisms underlying synapse-microglia interactions in guiding microglial homeostasis.

Repopulating cells recapitulate functional features of endogenous microglia

Although microglial repopulation following depletion can restore microglia numbers, the question of whether these replacement cells can fully recapitulate the functional features of endogenous microglia had not been previously addressed (*3*). Live-cell imaging in the retina showed that the constitutive process motility demonstrated by repopulated microglia was quantitatively indistinguishable from that demonstrated by endogenous microglia. Because this functional feature of dynamic process behavior, which is conserved across retina and brain compartments (*23*, *31*), is regulated by neuronal signals (*15*, *24*) and, in turn, can modulate the structure and function of contacted synapses (*32*), this finding indicates that repopulating microglia are not merely relocated in the niches previously occupied by endogenous microglia but are functionally

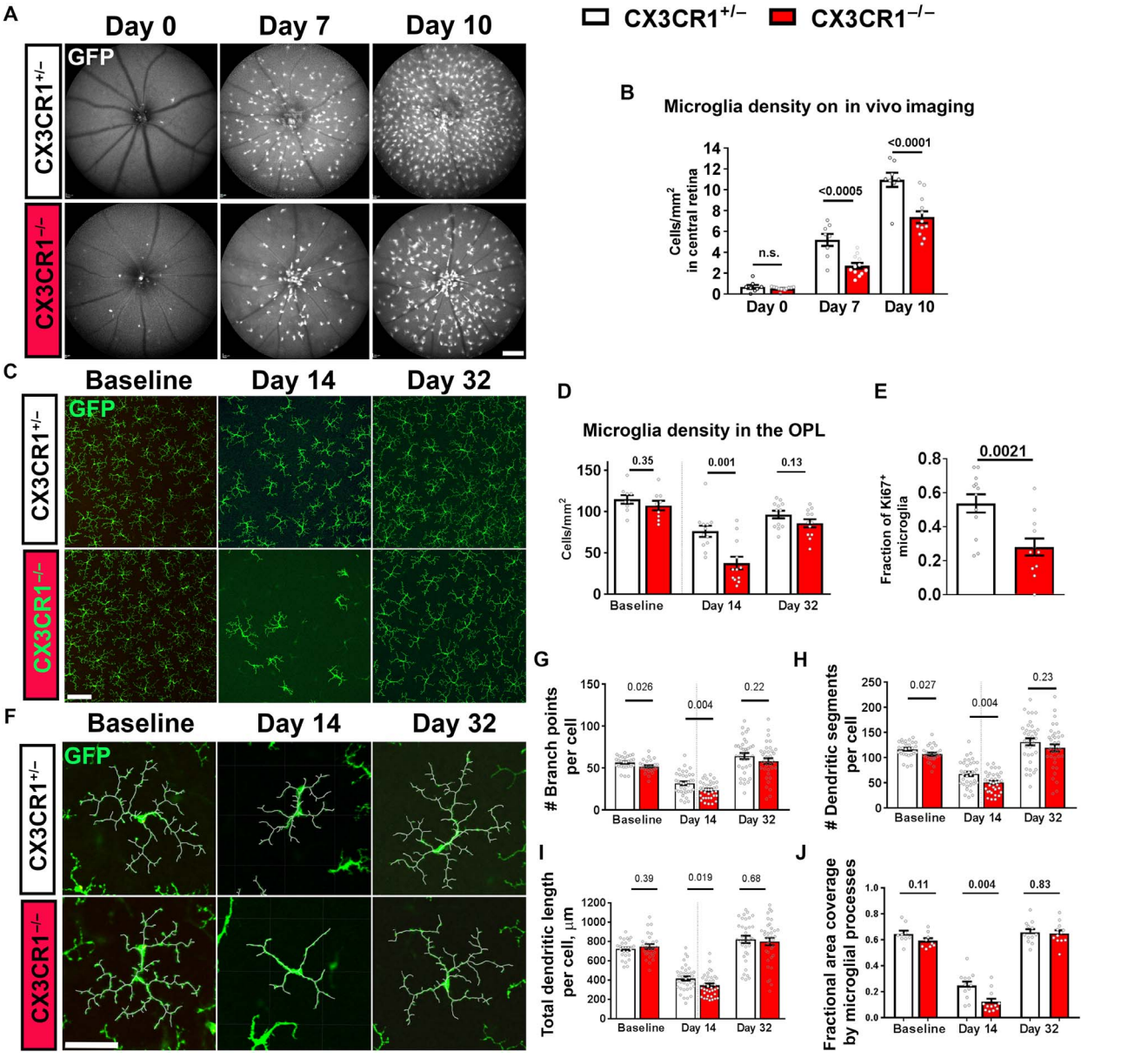

Fig. 6. Microglia repopulation following depletion in the retina is slowed in CX3CR1 deficiency. Eight-week-old signaling-deficient *CX3CR1*$^{-/-}$ mice and their signaling-sufficient *CX3CR1*$^{+/-}$ littermates were subjected to PLX5622-mediated microglial depletion for 7 days and allowed to undergo microglial repopulation. (**A** and **B**) Microglial repopulation in the central retina was followed for the first 10 days of repopulation using in vivo fundus imaging of GFP-labeled microglia and compared between *CX3CR1*$^{+/-}$ and *CX3CR1*$^{-/-}$ littermates. The numbers of residual microglia were comparable in the two groups following depletion (day 0), but CX3CR1-deficient microglia demonstrated significantly slower recovery of microglial numbers at days 7 and 10 ($n = 8$ *CX3CR1*$^{+/-}$ and 12 *CX3CR1*$^{-/-}$ animals). (**C** and **D**) Microglial repopulation in the OPL of the mid-peripheral retina was compared in flat-mounted retina. Although microglial densities, revealed by GFP expression, were similar between the two genotypes at baseline, the recovery of microglial density was slower in *CX3CR1*$^{-/-}$ animals at day 14. At day 32, microglial densities were comparable between the genotypes and approached baseline ($n = 9$, 12, and 12 imaging fields from 3, 4, and 4 animals for each genotype at baseline, day 14, and day 32, respectively). (**E**) The proportion of repopulating microglia undergoing active replication at day 14, as measured by Ki67 immunopositivity, was significantly lower in *CX3CR1*$^{-/-}$ animals ($n = 12$ imaging fields in 4 animals for each genotype group). (**F** to **J**) Morphological analyses of GFP-expressing repopulating microglia in the OPL showed that while the morphology was partially similar between genotypes at baseline, the maturation of ramified morphology at day 14 was significantly slower in *CX3CR1*$^{-/-}$ animals. By day 32, morphology in both genotypes was comparable and recovered to baseline levels. Besides, the fractional area coverage of synaptic laminar by *CX3CR1*$^{-/-}$ microglia was significantly lower at day 14. (G to I) $n = 27$, 36, and 36 cells [(J) $n = 9$, 12, and 12 imaging fields)] from 3, 4, and 4 animals for each genotype at baseline, day 14, and day 32, respectively. (A to D and J) One-way ANOVA with Sidak's multiple-comparisons test, (E) unpaired *t* test with Welch's correction, and (G to I) Kruskal-Wallis test with Dunn's multiple-comparisons test. Scale bars, 250 µm (A), 100 µm (C), and 50 µm (F).

integrated into the system of microglia-neuron interactions. Repopulating microglia demonstrated identical morphological responses to extracellular ATP as endogenous microglia, indicating that they express similar membrane-bound ATP-responsive receptors (*33*) and intracellular mediators that engage the cytoskeletal elements responsible for process motility (*34*). We also found that microglial responses to in vivo photoreceptor injury, in terms of activation, migration, and up-regulation of inflammatory cytokines, were similar between repopulating and

endogenous microglia, indicating a restoration of the ability to sense and respond to damage-associated molecular pattern molecules (*35*). Although there is some controversy as to whether microglia play a required role in the constitutive maintenance of synaptic function in the adult brain (*5*, *20*), we have previously found that microglia are indeed required in the adult retina to achieve optimal synaptic structure and function to mediate normal ERG responses to light. These responses otherwise decline progressively with increasing duration of microglial depletion (*10*). Significantly, we demonstrated here that repopulating microglia can restore or forestall decrements in ERG function, providing evidence that they can take over the homeostatic functions of endogenous microglia required for normal functioning in the adult retina. Our findings here showed that the precise recapitulation of microglial distribution and morphology underlying the repopulation response is correlated with the restoration of preexisting constitutive microglial functions in the adult retina.

Regulation of microglial repopulation by CX3CL1-CX3CR1 signaling

The coordinated nature of proliferation and migration of repopulating microglia in the retina suggests the role of neuronal cues that can serve to regulate and guide the process to fully reestablish microglial homeostasis. In the brain, IL-1R signaling has been found to regulate microglial repopulation; inhibition of signaling resulted in delayed repopulation and morphological ramification (*4*). We found here that neuron-to-microglia communication in the form of CX3CL1-CX3CR1 signaling in the retina plays an important regulatory role; CX3CR1 deficiency delayed microglial repopulation by decreasing cell proliferation and hindered the morphological maturation of repopulating cells, whereas exogenous CX3CL1 administration conversely accelerated the rate of repopulation through increased CX3CR1-mediated signaling. In the retina, where CX3CL1 is constitutively expressed by retinal neurons in the inner layers of the retina (*14*), CX3CL1-CX3CR1 signaling has been documented to mediate multiple aspects of microglial physiology, including process motility, microglial localization, and regulation of activation (*15*, *16*), indicating that it is an influential and ongoing mode of neuron-microglia communication in the adult retina. Our results here reveal that CX3CL1-CX3CR1 signaling plays a novel role in regulating microglial homeostasis through potentiating microglial proliferation and morphological maturation. These functions of CX3CL1-CX3CR1 signaling are likely mechanistically related to its developmental role in regulating microglial colonization of the neonatal hippocampus (*12*) and of barrel centers in the somatosensory cortex (*36*). Similar to the developing somatosensory cortex, there is a spatial correspondence between the concentration of CX3CL1 expression in the inner retina and the zone in which microglial repopulation originates, suggesting that CX3CL1 may act as a local trophic factor for microglial proliferation (*37*) and as a chemotactic molecule for guiding migration of repopulating microglia. Alternatively, CX3CL1-CX3CR1 signaling may exert a general permissive influence that potentiates microglial responsiveness to other guidance cues such as ATP and other activity-dependent signals (*38*). Because CX3CR1 deficiency resulted in a delay in the progress of repopulation, but did not prevent full repopulation from taking place, additional regulatory factors, possibly other chemokines acting in concert with CX3CL1-CX3CR1 signaling, are likely involved. Knowledge of the mechanisms governing the homeostatic regulation of microglia in adult systems will be central to the formulation of novel immunomodulatory treatments (for example, those involving "microglia replacement") (*39*, *40*) in the treatment of CNS disorders.

Together, our findings here demonstrate that microglial homeostasis in the retina is achieved through a coordinated process involving the in situ proliferation and migration of residual cells that is guided by intraretinal cues to recover not only the full structural organization of the original cells but also the constitutive microglial functions of immunosurveillance and synaptic maintenance. This homeostatic process is subject to regulation by CX3CL1-CX3CR1 signaling, which potentiates microglial proliferation and morphological maturation, underscoring the central role of neuron-microglia communications underlying immune homeostasis in the CNS.

MATERIALS AND METHODS

Experimental animals

Experiments were conducted according to protocols approved by the National Eye Institute Animal Care and Use Committee and adhered to the Association for Research in Vision and Ophthalmology statement for the use of animals in ophthalmic and vision research. Animals were housed in a National Institutes of Health (NIH) animal facility under a 12-hour light/12-hour dark cycle with food ad libitum. Transgenic mice in which the *CX3CR1* gene was replaced by a sequence encoding Cre recombinase with a tamoxifen-dependent estrogen ligand-binding domain (*CX3CR1*^{CreER} mice, provided by W.-B. Gan, Skirball Institute) (*20*) were crossed with mice containing a *flox-STOP-flox DTA* gene cassette in the *Rosa26* locus (The Jackson Laboratory, catalog #009669) (*Rosa26-flox-STOP-flox–DTA* mice) to obtain mice heterozygous in both loci (designated *CX3CR1*^{CreER}*-DTA* mice). *CX3CR1*^{CreER} mice were also crossed with mice harboring a loxP-flanked STOP cassette preventing the transcription of a CAG promoter-driven RFP variant (tdT) that had been inserted into the Gt(ROSA)26Sor locus (The Jackson Laboratory, catalog no. 007914). These animals (designated *CX3CR1*$^{CreER/+}$*:tdT* mice) were used in fate mapping experiments to distinguish monocytes from cells derived from endogenous microglia. Transgenic mice in which one copy of the *CX3CR1* gene was replaced by sequences coding for GFP (designated *CX3CR1*$^{+/GFP}$ mice, The Jackson Laboratory, catalog no. 005582) were used for ex vivo and in vivo live imaging of retinal microglial behavior. Transgenic mice in which one copy of the *CCR2* gene was replaced by sequences coding for RFP (designated *CCR2*$^{+/RFP}$ mice; The Jackson Laboratory, catalog no. 017586) were crossed with *CX3CR1*^{CreER}*-DTA* mice to generate *CX3CR1*^{CreER}*-DTA:CCR2*$^{+/RFP}$ mice; these mice were used to detect the infiltration of CCR2-expressing monocytes into the retina following microglial depletion.

Models for microglial depletion-repopulation in the retina

Two experimental models for the depletion and repopulation of microglia in the retina were employed. The first model involved the use of *CX3CR1*^{CreER}*-DTA* mice in which oral tamoxifen administration via gavage (500 mg/kg dose in a 20 mg/ml solution of corn oil) induced the expression of DTA specifically in CX3CR1-expressing cells, resulting in their ablation (*10*). Animals were administered two oral doses of tamoxifen, each 1 day apart, and then allowed to undergo microglial repopulation; the day of the final tamoxifen dose was designated day 0 of the repopulation phase. The second model involved the dietary administration of PLX5622 (Plexxikon), a potent and selective inhibitor of the CSF1R, previously demonstrated to deplete microglia in the brain (*21*). Animals were placed on a rodent chow containing PLX5622 (at 1200 parts per million) for 7 days to induce microglial depletion in the retina and then switched back to a control standard chow to allow for repopulation; the first day of control diet resumption was designated day 0 of the repopulation phase.

Immunohistochemical analysis of retinal tissue

Mice were euthanized by CO_2 inhalation, and their eyes were removed. Enucleated eyes were dissected to form posterior segment eyecups that were then fixed in 4% paraformaldehyde in PBS for 2 to 4 hours at 4°C. Eyecups were either processed for vibratome sectioning (100-μm-thick sections; VT1000, Leica) or dissected to form retinal flat-mounts. Flat-mounted retinas or retinal sections were blocked for 4 hours in blocking buffer containing 10% normal donkey serum and 0.5% Triton X-100 in PBS at room temperature. Primary antibodies, which included Iba1 (1:500; Wako, catalog no. 019-19741), nestin (1:200; Santa Cruz Biotechnology, catalog no. sc-33677), and CD68 (1:400; Bio-Rad, catalog no. MCA1957), were diluted in blocking buffer and applied overnight for sections and for 24 hours for flat-mounts at 4°C on a shaker. Experiments in which primary antibodies were omitted served as negative controls. After washing in 1× PBS with 0.5% Triton X-100, sections were incubated overnight with secondary antibodies (Alexa Fluor 488– or Alexa Fluor 568–conjugated anti-rabbit, mouse, or rat immunoglobulin G) and DAPI (1:500; Sigma-Aldrich) to label cell nuclei. IB4, conjugated to Alexa Fluor 568 (1:100; Life Technologies), was used to detect activated microglia. Ki67, conjugated to eFluor660 (1:50; eBioscience, catalog no. 53-3249-82), was used to detect proliferating cells. Stained retinal flat-mounts and sections were imaged with confocal microscopy (Olympus FluoView 1000 or Zeiss LSM 880). For analysis at high magnification, multiplane z series were collected using a 20× or 40× objective; each z series spanned from the vitreal surface to the OPL for retinal flat-mounts, and over a depth of 20 μm for retinal sections, with each section spaced 1 to 2.5 μm apart. Confocal image stacks were viewed and analyzed with FV10-ASW 4.2 Viewer Software (Olympus), Zen software (Zeiss), and/or ImageJ (NIH). To visualize microglial distributions over the entire retina, tiled images of retinal flat-mounts were obtained under a 10× objective using epifluorescence microscopy and stitched together with image analysis software (Axio Imager Z1, Carl Zeiss Microscopy).

Image analysis

To analyze the total numbers of microglia in the retina, manual counts of $Iba1^+$ cells were performed over the entire retina in flat-mounted specimens. To determine the total area occupied by repopulating microglia, retinal areas containing microglia were circumscribed and measured using computer-assisted software (ImageJ). Microglial counts in the separate retinal lamina (IPL, OPL, and interplexiform region) were performed manually from high-magnification image stacks captured at consistent retinal regions of interest (ROIs) positioned midway between the optic nerve and the retinal periphery. Three-dimensional morphological analyses of microglia were performed using computer-assisted segmentation of microglial processes [Filament Tracer module and the convex hull feature, Imaris software (V8.2.1), Bitplane] for individual cells located in the same ROIs. The following were the morphological parameters that were quantitated: (i) number of branching points in the dendritic field of individual microglial cells, (ii) total dendritic process length of a microglial cell, and (iii) mean volume occupied per cell (the three-dimensional volume subtended by a single microglial dendritic field). Fractional occupation by IB4 and CD68 in $Iba1^+$ microglia was evaluated in similarly positioned ROIs by computing the fraction of immunopositive pixels occurring within the area of Iba1 immunopositivity using standardized imaging parameters.

In vivo scanning laser ophthalmoscope imaging of repopulating retinal microglia

Two-month-old *CX3CR1*$^{+/GFP}$ and *CX3CR1*$^{CreER/+}$-*tdT* mice were subjected to PLX5622-mediated microglial depletion and allowed to undergo microglial repopulation. At days 5 and 12 of the repopulation process, animals were subjected to pupillary dilation with topical tropicamide (1%; Alcon) and phenylephrine (10%; Alcon) and anesthetized using isoflurane. In vivo fluorescence fundus imaging of GFP-labeled retinal microglia was performed using a scanning laser ophthalmoscope (SLO) (Spectralis, Heidelberg Engineering) with 488- or 518-nm laser illumination. A 55° wide-angle lens was used to visualize the posterior pole. To monitor the progressive migration of repopulating cells, fundus images were obtained every 1 to 1.5 hours in recording sessions of 5- to 9-hour duration. Consecutive fundus images were aligned, and migratory movements of individual retinal microglial cells were tracked and quantitated using NIH ImageJ software.

Fate mapping of the endogenous microglia

Two-month-old *CX3CR1*$^{CreER/+}$-*tdT* mice were subjected to two doses of tamoxifen administration by gavage (500 mg/kg per dose) to induce tdT expression in all CX3CR1-expressing myeloid cells, including microglia and systemic monocytes. These animals were then housed under standard conditions for another 3 months during which systemic monocytes were allowed to be completely turned over and replaced by tdT^- cells, while longer-lived microglia in the retina remained tdT^+ (*20*). Depletion by PLX5622 administration (for 7 days) was induced following monocyte turnover; microglial repopulation was then allowed to occur following the resumption of a control diet. Repopulating retinal microglia were assessed for tdT expression with longitudinal in vivo fundus imaging using SLO (green fluorescence with a 518-nm laser and a 55° wide-angle lens) at days 0, 7, and 30 of repopulation and in confocal microscopic immunohistochemical analyses of flat-mounted retinal tissue at day 30.

Ex vivo time-lapse confocal imaging of microglial behavior

Two-month-old *CX3CR1*$^{+/GFP}$ mice were subjected to PLX5622-mediated microglial depletion for 7 days and allowed to undergo microglial repopulation for 2 months. Retinal explants were prepared from these animals and from age-matched *CX3CR1*$^{+/GFP}$ mice that had not been subjected to microglia depletion, as previously described (*23*). Baseline dynamic behavior of repopulated microglia versus endogenous microglia was monitored and recorded using time-lapse confocal microscopy; responses to the addition of exogenous ATP (5 mM in Ringer's solution, Sigma-Aldrich) into the imaging chamber were also recorded. Time-lapse image stacks were captured every 24 s for up to 30 min. Two-dimensional time-lapse movies were created from maximum intensity projections in the *z* dimension and aligned in the *x*-*y* plane using the StackReg plugin of NIH ImageJ software. Rates of process extension and retraction of individual microglial cells were measured as previously described (*24*).

Light-induced model of retinal injury

Three- to four-month-old wild-type C57Bl6 animals containing repopulated microglia and nondepleted control animals were subjected to a light-induced model of retinal injury in which short-term light exposure resulted in progressive photoreceptor injury and degeneration, as previously described (*26*). Microglial responses to photoreceptor injury were evaluated by immunohistochemistry in retinal sections and by cytokine analysis in retinal tissue 7 days following light injury.

Measurement of cytokine levels in retinal tissue

Dissected mouse retinas were lysed by trituration in protein lysate buffer (Complete Ultra; Roche) with proteinase inhibitor mixture (Calbiochem) at 4°C. After sonication and centrifugation, protein concentration was

measured (BCA Protein Assay Kit, Pierce). Cytokine levels were determined using a Milliplex VR assay kit (Milliplex MAP mouse cytokine/chemokine magnetic bead panel; #MCYTOMAG-70K, Millipore) and the Luminex MAGPIX system with data analysis using xPONENT 4.2 software (Luminex).

Gene expression analysis

For whole transcriptome analysis, retinas from both eyes of the following groups of *CX3CR1*^{CreER}*-DTA* mice were collected: (i) animals not subjected to microglial depletion (controls) and animals that were subjected to depletion and allowed to undergo repopulation for (ii) 5 days, (iii) 15 days, and (iv) 30 days. After harvesting, all samples were frozen before RNA extraction using the Qiagen RNA Mini Kit with RNase (ribonuclease)–free DNase (deoxyribonuclease) I digestion. RNA quality and quantity were evaluated using BioAnalyzer 2100 with the RNA 6000 Nano Kit (Agilent Technologies). RNA sequencing libraries were constructed from 1 μg of total RNA using a modified TruSeq RNA Sample preparation kit protocol. Pass-filtered reads were mapped using TopHat v2.0.11 (*41*) and aligned to National Center for Biotechnology Information mouse reference genome Build 38/mm10. The count table of the gene features was obtained using HTSeq. EdgeR was used to compute differential expression analysis and to calculate FPKM (fragments per kilobase of exon per million fragments mapped) values.

ERG analysis

ERGs were recorded at baseline just before microglial depletion and at different time points following microglial depletion/repletion using an Espion E^2 system (Diagnosys). Mice were dark-adapted overnight and prepared for recording in darkness under dim-red illumination. Mice were anesthetized with intraperitoneal ketamine (90 mg/kg) and xylazine (8 mg/kg) and were topically administered tropicamide (1%; Alcon) and phenylephrine (2.5%; Alcon) for pupillary dilation and proparacaine hydrochloride (0.5%; Alcon) for topical anesthesia. Flash ERG recordings were obtained simultaneously from both eyes with gold wire loop electrodes. The reference electrode was placed in the mouth and the ground subdermal electrode was placed at the tail. ERG responses were obtained at increasing light intensities over the 1×10^{-4} to 10 cd·s/m^2 or 0.3 to 100 cd·s/m^2 range, respectively, under dark- or light-adapted conditions. The stimulus interval between flashes varied from 5 s at the lowest stimulus strengths to 60 s at the highest ones. Two to 10 responses were averaged depending on flash intensity. ERG signals were sampled at 1 kHz and recorded with 0.3-Hz low-frequency and 300-Hz high-frequency cutoffs. Analysis of a-wave and b-wave amplitudes was performed using customized ERG Data Analyzer software (v2.2). The a-wave amplitude was measured from the baseline to the negative peak and the b-wave was measured from the a-wave trough to the maximum positive peak.

Tissue preparation for electron microscopy analysis

The specimens were prepared for transmission electron microscopy. Briefly, tissues were fixed in PBS-buffered glutaraldehyde (2.5% at pH 7.4) and PBS-buffered osmium tetroxide (0.5%), and embedded in epoxy resin. Thin sections (90 nm) were collected on 200-mesh copper grids, dried for 24 hours, and double-stained with uranyl acetate and lead citrate. Sections were viewed and photographed with a JEOL JM-1010 electron microscope.

Intravitreal delivery of CX3CL1

Two- to three-month-old *CX3CR1*$^{+/GFP}$ and *CX3CR1*$^{+/GFP}$ mice were administered the PLX5622 diet for 7 days to induce microglial depletion in the retina and then allowed to undergo repopulation. At day 3 of the repopulation period (following cessation of the PLX5622 diet), exogenous full-length recombinant mouse CX3CL1 in PBS (R&D Systems, #472-FF/CF; 1.5 μl injection of 66 ng/μl solution, final vitreous concentration of 24.75 ng/μl in PBS) was injected intravitreally into one eye and the contralateral control eye was injected with an equal volume and concentration of heat-inactivated (95°C for 45 min) CX3CL1 in PBS. Animals were evaluated with in vivo fluorescence fundus imaging at day 7, and the experimental eyes were harvested for analysis thereafter. Retinal flat-mounts were prepared and were imaged with confocal microscopy (Zeiss LSM 880). The density of repopulating cells was assessed by manual counting; for in vivo fundus images, all microglia within the central 55° field were counted; for histological analyses of retinal flat-mounts, cell counts were performed in 20× imaging fields captured in the central retina, which was defined as the area circumscribed around the optic nerve by a radius equal to one-third of the distance between the optic nerve and the retinal periphery (3 to 4 ROIs per retinal flat mount).

Statistical analysis

All data were analyzed using statistical software (GraphPad Software). A normality test (D'Agostino and Pearson) was used to analyze the distribution of all data sets. For comparisons involving two data columns, *t* tests or nonparametric tests (Mann-Whitney) were used, depending on whether the data followed a Gaussian distribution as determined by normality tests. For comparisons involving three or more data columns, a one-way ANOVA (with Dunnett's multiple-comparisons test) was used if the data followed a Gaussian distribution and a nonparametric Kruskal-Wallis test (with Dunn's multiple-comparisons test) was used if it did not. A two-way ANOVA and Sidak's multiple-comparisons test were used to compare ERG data and repopulation curves from different groups of animals. Paired data sets were analyzed with a paired *t* test. A P value <0.05 was set as the basis for rejecting the null hypothesis. In all graphical representations, the error bars indicate SE unless otherwise indicated.

SUPPLEMENTARY MATERIALS

Supplementary material for this article is available at http://advances.sciencemag.org/cgi/content/full/4/3/eaap8492/DC1

fig. S1. Microglial repopulation in the adult wild-type mouse retina in a pharmacological (PLX5622) model of microglial depletion demonstrates a center-to-peripheral, vitreal-to-scleral progression.

fig. S2. Repopulating Iba1$^+$ cells undergo progressive morphological maturation to recapitulate morphologies of endogenous retinal microglia in the *CX3CR1*^{CreER}-DTA model of microglial depletion.

fig. S3. Repopulating Iba1$^+$ cells undergo progressive morphological maturation to recapitulate morphologies of endogenous retinal microglia in the PLX5622-mediated model of microglial depletion.

fig. S4. Repopulating Iba1$^+$ cells demonstrate transient expression of markers of microglial activation and replication in the *CX3CR1*^{CreER}-DTA model of microglial depletion.

fig. S5. Repopulating Iba1$^+$ cells demonstrate transient expression of markers of activation and replication in the PLX5622-induced model of microglial depletion.

fig. S6. Microglial repopulation rescues deterioration of retinal function induced by microglia depletion in the PLX5622 model.

fig. S7. Intravitreal delivery of exogenous CX3CL1 accelerates microglial repopulation.

fig. S8. Estimation of cell proliferation dynamics during the repopulation process: Proliferation rates of residual microglia are sufficient to regenerate cells observed during the repopulation process.

movie S1. Dynamic migration and in situ replication of repopulating microglia in the retina.

movie S2. Dynamic migration and replication of repopulating microglia slow down as microglial density increases in the retina.

movie S3. Repopulating microglia demonstrate dynamic motility in their processes at baseline and in response to exogenous ATP that are similar to that in endogenous microglia.

REFERENCES AND NOTES

1. T. L. Tay, D. Mai, J. Dautzenberg, F. Fernández-Klett, G. Lin, Sagar, M. Datta, A. Drougard, T. Stempfl, A. Ardura-Fabregat, O. Staszewski, A. Margineanu, A. Sporbert, L. M. Steinmetz, J. A. Pospisilik, S. Jung, J. Priller, D. Grün, O. Ronneberger, M. Prinz, A new fate mapping system reveals context-dependent random or clonal expansion of microglia. *Nat. Neurosci.* **20**, 793–803 (2017).
2. K. Kierdorf, M. Prinz, Microglia in steady state. *J. Clin. Invest.* **127**, 3201–3209 (2017).
3. A. Waisman, F. Ginhoux, M. Greter, J. Bruttger, Homeostasis of microglia in the adult brain: Review of novel microglia depletion systems. *Trends Immunol.* **36**, 625–636 (2015).
4. J. Bruttger, K. Karram, S. Wörtge, T. Regen, F. Marini, N. Hoppmann, M. Klein, T. Blank, S. Yona, Y. Wolf, M. Mack, E. Pinteaux, W. Müller, F. Zipp, H. Binder, T. Bopp, M. Prinz, S. Jung, A. Waisman, Genetic cell ablation reveals clusters of local self-renewing microglia in the mammalian central nervous system. *Immunity* **43**, 92–106 (2015).
5. M. R. P. Elmore, A. R. Najafi, M. A. Koike, N. N. Dagher, E. E. Spangenberg, R. A. Rice, M. Kitazawa, B. Matusow, H. Nguyen, B. L. West, K. N. Green, Colony-stimulating factor 1 receptor signaling is necessary for microglia viability, unmasking a microglia progenitor cell in the adult brain. *Neuron* **82**, 380–397 (2014).
6. Y. Yao, S. Echeverry, X. Q. Shi, M. Yang, Q. Z. Yang, G. Y. F. Wang, J. Chambon, Y. C. Wu, K. Y. Fu, Y. De Koninck, J. Zhang, Dynamics of spinal microglia repopulation following an acute depletion. *Sci. Rep.* **6**, 22839 (2016).
7. D. Kokona, N. Schneider, H. Giannakaki-Zimmermann, J. Jovanovic, A. Ebneter, M. Zinkernagel, Noninvasive quantification of retinal microglia using widefield autofluorescence imaging. *Invest. Ophthalmol. Vis. Sci.* **58**, 2160–2165 (2017).
8. J. G. Robson, H. Maeda, S. M. Saszik, L. J. Frishman, In vivo studies of signaling in rod pathways of the mouse using the electroretinogram. *Vision Res.* **44**, 3253–3268 (2004).
9. J. Boya, J. Calvo, A. L. Carbonell, Appearance of microglial cells in the postnatal rat retina. *Arch. Histol. Jpn.* **50**, 223–228 (1987).
10. X. Wang, L. Zhao, J. Zhang, R. N. Fariss, W. Ma, F. Kretschmer, M. Wang, H. h. Qian, T. C. Badea, J. S. Diamond, W.-B. Gan, J. E. Roger, W. T. Wong, Requirement for microglia for the maintenance of synaptic function and integrity in the mature retina. *J. Neurosci.* **36**, 2827–2842 (2016).
11. K. Biber, J. Vinet, H. W. G. M. Boddeke, Neuron-microglia signaling: Chemokines as versatile messengers. *J. Neuroimmunol.* **198**, 69–74 (2008).
12. R. C. Paolicelli, G. Bolasco, F. Pagani, L. Maggi, M. Scianni, P. Panzanelli, M. Giustetto, T. A. Ferreira, E. Guiducci, L. Dumas, D. Ragozzino, C. T. Gross, Synaptic pruning by microglia is necessary for normal brain development. *Science* **333**, 1456–1458 (2011).
13. F. Pagani, R. C. Paolicelli, E. Murana, B. Cortese, S. Di Angelantonio, E. Zurolo, E. Guiducci, T. A. Ferreira, S. Garofalo, M. Catalano, G. D'Alessandro, A. Porzia, G. Peruzzi, F. Mainiero, C. Limatola, C. T. Gross, D. Ragozzino, Defective microglial development in the hippocampus of *Cx3cr1* deficient mice. *Front. Cell. Neurosci.* **9**, 111 (2015).
14. M. Zieger, P. K. Ahnelt, P. Uhrin, CX3CL1 (fractalkine) protein expression in normal and degenerating mouse retina: In vivo studies. *PLOS ONE* **9**, e106562 (2014).
15. K. J. Liang, J. E. Lee, Y. D. Wang, W. Ma, A. M. Fontainhas, R. N. Fariss, W. T. Wong, Regulation of dynamic behavior of retinal microglia by CX3CR1 signaling. *Invest. Ophthalmol. Vis. Sci.* **50**, 4444–4451 (2009).
16. C. Combadière, C. Feumi, W. Raoul, N. Keller, M. Rodéro, A. Pézard, S. Lavalette, M. Houssier, L. Jonet, E. Picard, P. Debré, M. Sirinyan, P. Deterre, T. Ferroukhi, S.-Y. Cohen, D. Chauvaud, J.-C. Jeanny, S. Chemtob, F. Behar-Cohen, F. Sennlaub, CX3CR1-dependent subretinal microglia cell accumulation is associated with cardinal features of age-related macular degeneration. *J. Clin. Invest.* **117**, 2920–2928 (2007).
17. M. Colonna, O. Butovsky, Microglia function in the central nervous system during health and neurodegeneration. *Annu. Rev. Immunol.* **35**, 441–468 (2017).
18. R. A. Rice, J. Pham, R. J. Lee, A. R. Najafi, B. L. West, K. N. Green, Microglial repopulation resolves inflammation and promotes brain recovery after injury. *Glia* **65**, 931–944 (2017).
19. C. M. Diaz-Araya, J. M. Provis, P. L. Penfold, F. A. Billson, Development of microglial topography in human retina. *J. Comp. Neurol.* **363**, 53–68 (1995).
20. C. N. Parkhurst, G. Yang, I. Ninan, J. N. Savas, J. R. Yates III, J. J. Lafaille, B. L. Hempstead, D. R. Littman, W.-B. Gan, Microglia promote learning-dependent synapse formation through brain-derived neurotrophic factor. *Cell* **155**, 1596–1609 (2013).
21. N. N. Dagher, A. R. Najafi, K. M. Neely Kayala, M. R. P. Elmore, T. E. White, R. Medeiros, B. L. West, K. N. Green, Colony-stimulating factor 1 receptor inhibition prevents microglial plaque association and improves cognition in 3xTg-AD mice. *J. Neuroinflammation* **12**, 139 (2015).
22. M. Mizutani, P. A. Pino, N. Saederup, I. F. Charo, R. M. Ransohoff, A. E. Cardona, The fractalkine receptor but not CCR2 is present on microglia from embryonic development throughout adulthood. *J. Immunol.* **188**, 29–36 (2012).
23. J. E. Lee, K. J. Liang, R. N. Fariss, W. T. Wong, Ex vivo dynamic imaging of retinal microglia using time-lapse confocal microscopy. *Invest. Ophthalmol. Vis. Sci.* **49**, 4169–4176 (2008).
24. A. M. Fontainhas, M. Wang, K. J. Liang, S. Chen, P. Mettu, M. Damani, R. N. Fariss, W. Li, W. T. Wong, Microglial morphology and dynamic behavior is regulated by ionotropic glutamatergic and GABAergic neurotransmission. *PLOS ONE* **6**, e15973 (2011).
25. G. W. Kreutzberg, Microglia: A sensor for pathological events in the CNS. *Trends Neurosci.* **19**, 312–318 (1996).
26. X. Wang, L. Zhao, Y. Zhang, W. Ma, S. R. Gonzalez, J. Fan, F. Kretschmer, T. C. Badea, H.-h. Qian, W. T. Wong, Tamoxifen provides structural and functional rescue in murine models of photoreceptor degeneration. *J. Neurosci.* **37**, 3294–3310 (2017).
27. M. K. Zabel, L. Zhao, Y. Zhang, S. R. Gonzalez, W. Ma, X. Wang, R. N. Fariss, W. T. Wong, Microglial phagocytosis and activation underlying photoreceptor degeneration is regulated by CX3CL1-CX3CR1 signaling in a mouse model of retinitis pigmentosa. *Glia* **64**, 1479–1491 (2016).
28. J. Han, R. A. Harris, X.-M. Zhang, An updated assessment of microglia depletion: Current concepts and future directions. *Mol. Brain* **10**, 25 (2017).
29. F. Sennlaub, C. Auvynet, B. Calippe, S. Lavalette, L. Poupel, S. J. Hu, E. Dominguez, S. Camelo, O. Levy, E. Guyon, N. Saederup, I. F. Charo, N. Van Rooijen, E. Nandrot, J.-L. Bourges, F. Behar-Cohen, J.-A. Sahel, X. Guillonneau, W. Raoul, C. Combadiere, $CCR2^+$ monocytes infiltrate atrophic lesions in age-related macular disease and mediate photoreceptor degeneration in experimental subretinal inflammation in *Cx3cr1* deficient mice. *EMBO Mol. Med.* **5**, 1775–1793 (2013).
30. N. H. Varvel, S. A. Grathwohl, K. Degenhardt, C. Resch, A. Bosch, M. Jucker, J. J. Neher, Replacement of brain-resident myeloid cells does not alter cerebral amyloid-β deposition in mouse models of Alzheimer's disease. *J. Exp. Med.* **212**, 1803–1809 (2015).
31. D. Davalos, J. Grutzendler, G. Yang, J. V. Kim, Y. Zuo, S. Jung, D. R. Littman, M. L. Dustin, W.-B. Gan, ATP mediates rapid microglial response to local brain injury in vivo. *Nat. Neurosci.* **8**, 752–758 (2005).
32. H. Wake, A. J. Moorhouse, S. Jinno, S. Kohsaka, J. Nabekura, Resting microglia directly monitor the functional state of synapses in vivo and determine the fate of ischemic terminals. *J. Neurosci.* **29**, 3974–3980 (2009).
33. S. Koizumi, K. Ohsawa, K. Inoue, S. Kohsaka, Purinergic receptors in microglia: Functional modal shifts of microglia mediated by P2 and P1 receptors. *Glia* **61**, 47–54 (2013).
34. A.-K. Persson, M. Estacion, H. Ahn, S. Liu, S. Stamboulian-Platel, S. G. Waxman, J. A. Black, Contribution of sodium channels to lamellipodial protrusion and Rac1 and ERK1/2 activation in ATP-stimulated microglia. *Glia* **62**, 2080–2095 (2014).
35. M. R. P. Elmore, R. J. Lee, B. L. West, K. N. Green, Characterizing newly repopulated microglia in the adult mouse: Impacts on animal behavior, cell morphology, and neuroinflammation. *PLOS ONE* **10**, e0122912 (2015).
36. M. Hoshiko, I. Arnoux, E. Avignone, N. Yamamoto, E. Audinat, Deficiency of the microglial receptor CX3CR1 impairs postnatal functional development of thalamocortical synapses in the barrel cortex. *J. Neurosci.* **32**, 15106–15111 (2012).
37. G. E. White, D. R. Greaves, Fractalkine: A survivor's guide: Chemokines as antiapoptotic mediators. *Arterioscler. Thromb. Vasc. Biol.* **32**, 589–594 (2012).
38. R. C. Paolicelli, K. Bisht, M.-. Tremblay, Fractalkine regulation of microglial physiology and consequences on the brain and behavior. *Front. Cell. Neurosci.* **8**, 129 (2014).
39. N. Cartier, C. A. Lewis, R. Zhang, F. M. Rossi, The role of microglia in human disease: Therapeutic tool or target? *Acta Neuropathol.* **128**, 363–380 (2014).
40. M. Karlstetter, R. Scholz, M. Rutar, W. T. Wong, J. M. Provis, T. Langmann, Retinal microglia: Just bystander or target for therapy? *Prog. Retin. Eye Res.* **45**, 30–57 (2015).
41. C. Trapnell, L. Pachter, S. L. Salzberg, TopHat: Discovering splice junctions with RNA-Seq. *Bioinformatics* **25**, 1105–1111 (2009).

Acknowledgments

Funding: The study was supported by the National Eye Institute Intramural Research Program. **Author contributions:** Conceptualization: Y.Z., L.Z., and W.T.W. Methodology: Y.Z., L.Z., X.W., W.M., H.-h.Q., R.N.F., J.Z., M. A.-A., J.E.R., and W.T.W. Investigation: Y.Z., L.Z., X.W., W.M., A.L., J.Z., J.E.R., and W.T.W. Resources: H.-h.Q., R.N.F., and W.T.W. Writing (original draft): Y.Z., L.Z., and W.T.W. Writing (review and editing): Y.Z., L.Z., X.W., W.M., H.-h.Q., R.N.F., J.Z., M.A.-A., J.E.R., and W.T.W. Funding acquisition: W.T.W. **Competing interests:** The authors declare that they have no competing interests. **Data and materials availability:** All data needed to evaluate the conclusions in the paper are present in the paper and/or the Supplementary Materials. PLX5622 can be provided by Plexxikon pending scientific review and a completed material transfer agreement. Requests for the compound should be submitted to plexxikondrug@plexxikon.com.

Submitted 1 September 2017
Accepted 12 February 2018
Published 21 March 2018
10.1126/sciadv.aap8492

Citation: Y. Zhang, L. Zhao, X. Wang, W. Ma, A. Lazere, H.-. Qian, J. Zhang, M. Abu-Asab, R. N. Fariss, J. E. Roger, W. T. Wong, Repopulating retinal microglia restore endogenous organization and function under CX3CL1-CX3CR1 regulation. *Sci. Adv.* **4**, eaap8492 (2018).